Journal of Inorganic Biochemistry 199 (2019) 110707

Contents lists available at ScienceDirect

Journal of Inorganic Biochemistry

journal homepage: www.elsevier.com/locate/jinorgbio

pH responsive histidin-2-ylidene stabilized gold nanoparticles

Adam J. Young[a], Constantin Eisen[b], Guilherme M.D.M. Rubio[b], Jia Min Chin[a,b,*], Michael R. Reithofer[b,*]

[a] Gray Centre for Advanced Materials, School of Mathematics and Physical Sciences, University of Hull, Cottingham Road, Hull HU6 7RX, UK
[b] Institute of Inorganic Chemistry, University of Vienna, Faculty of Chemistry, Währinger Strasse 42, 1090 Vienna, Austria

ARTICLE INFO

Keywords:
N-Heterocyclic carbene
Gold nanoparticles
pH response

ABSTRACT

N-Heterocyclic carbene-stabilized metal nanoparticles have drawn much attention over the last decade due their strong carbon metal bond. Although several reports show increased stability of such N-heterocyclic carbene-stabilized metal nanoparticles, only limited examples of water-soluble N-heterocyclic carbene stabilized metal nanoparticles are known to date. However, water dispersibility and stability in biologically relevant solvents would be a prerequisite for any biological applications. Drawing from the natural amino acid chiral pool, L-histidine was utilized for preparing chiral NHC ligands in the synthesis of water soluble NHC-stabilized gold nanoparticles. For this purpose, *N*-acetyl-L-histidine ethyl ester was converted into its imidazolium salt either using methyl iodide or 2-iodopropane as alkylation agent. Subsequent reaction of the imidazolium salt with [Au(SMe_2)Cl] yielded the corresponding organometallic gold chloride complex. Histidine-2-ylidene stabilized gold nanoparticles were first generated in organic solvents; the histidine derived capping ligand bore ethyl ester moieties which were saponified, affording water soluble pH-responsive NHC-stabilized gold nanoparticles. These gold nanoparticles show remarkable stability in aqueous solutions, with gold nanoparticle solutions remaining stable after months of storage.

1. Introduction

The interest in nanoparticles (NPs) has increased substantially, due to their potential applications in material science, medicine and catalysis [1–5]. Amongst the wide array of nanoparticles, gold nanoparticles (AuNPs), in particular, are promising candidates for various biomedical applications such as imaging, sensing, drug delivery, and photothermal therapy [6–11], thanks to their unique optical properties, high surface area and biocompatibility. Such applications expose the AuNPs to variable environmental conditions such as, temperature, redox potential, pH, and chemical diversity. Stabilizing ligands are therefore required to provide solubility and long-term stability to the AuNPs in such conditions, which are essential for safety and reliability [12,13]. Although thiols have been traditionally used for the stabilization of AuNPs, the S—Au bond is not completely inert, limiting long term stability of such AuNPs [14–16]. As such, expanding the toolbox of functional surface anchors will provide unique opportunities for the construction of novel AuNP interfaces with greater stability.

Recent interest has focused on the use of N-heterocyclic carbenes (NHCs) as alternatives to thiols for the functionalization of AuNPs [17–22]. The charge neutral, electron rich NHCs form a coordination bond with the metallic surface, the strength of which is crucial to NP stability, allowing NPs to retain their surface ligands, maintain their sizes and their corresponding size-dependent properties. Despite the rich potential of AuNPs for biological applications, the use of NHC-stabilized AuNPs for biological systems has hardly been explored. For use in biological systems, NPs must possess solubility in aqueous media and stability under biological conditions. However, to date, there are only limited examples of water-dispersible NHC-stabilized metal NPs [19,23–26]. For example, Ravoo and Glorius reported the preparation of water soluble NHC-stabilized metal NPs for catalytic reactions, including water soluble Pd and Au NPs stabilized by bidentate hybrid NHC thioether ligands [19,26]. These NPs showed good pH stability in aqueous solutions, although no stability tests were undertaken in biological media. Johnson *et al.* reported on AuNPs stabilized with a polyethylene glycol (PEG)-modified NHC ligand [23]. The PEGylated NPs were found to have high stability across a range of pH values and good stability under biologically relevant electrolyte concentrations. Crudden et al. recently reported NHC-stabilized AuNPs which exploit a simple carboxylic acid moiety to enable water solubility [24]. The resulting AuNPs were stable in various biological media and in a wide range of pH solutions but did not demonstrate any pH responsivity.

* Corresponding author.
E-mail addresses: j.chin@hull.ac.uk (J.M. Chin), michael.reithofer@univie.ac.at (M.R. Reithofer).

https://doi.org/10.1016/j.jinorgbio.2019.110707
Received 1 March 2019; Received in revised form 25 April 2019; Accepted 2 May 2019
Available online 10 May 2019

Further, the smaller AuNPs were reported to have limited stability in aqueous solutions.

AuNPs with pH response are of particular interest when considering the use of AuNPs for imaging purposes. Kim *et al.* have reported the use of thiol functionalized, pH responsive 'smart' AuNPs as image contrast agents for signal amplification in photoacoustic imaging of cancer cells [27]. The reported 'smart' AuNPs can respond to mild acidic environments, such as in cancer cell environments, and rapidly aggregate due to ligand hydrolysis. However, this aggregation is irreversible. In addition, Wong et al. reported thiol derived AuNPs that exhibit a pH response when exposed to the acidic conditions of tumor environments, enhancing their capabilities as photoacoustic contrast agents [28]. These recent reports demonstrate the potential and possible applications for pH responsive AuNPs.

In light of the above considerations, we set out to prepare water soluble and reversibly pH responsive AuNPs with enhanced stability by utilizing an NHC-based, amino acid derived ligand bearing a free carboxylic acid moiety. By exploiting an amino acid as a stabilizing ligand, the resulting AuNPs are expected to display increased biocompatibility. We report here on histidin-2-ylidene stabilized gold nanoparticles which display excellent stability under various aqueous conditions. Due to the potential importance and increased stability of NHC-stabilized NPs for biomedical applications, the need to access water-soluble and biocompatible structures cannot be overstated.

2. Materials and methods

2.1. Chemicals

All experiments were performed in air except for the synthesis of [**2a** and **2b**] which were performed under a nitrogen atmosphere using Schlenk techniques. *N*-Acetyl-L-histidine monohydrate was purchased from Tokyo Chemical Industry, sodium borohydride was purchased from Lancaster chemicals, potassium carbonate, iodopropane and methyl iodide were purchased from Fluorochem, trimethylsilyl chloride (TMSCl), chloroauric acid and borane tert-butylamine complex were purchased from Alfa Aesar, acetonitrile (MeCN), dichloromethane (DCM), tetrahydrofuran (THF), pentane and diethyl ether were purchased from VWR chemicals. All purchased chemicals were used as received. Chloro(dimethyl sulfide) gold was synthesized according to literature procedure [29].

^{1}H and ^{13}C NMR spectra were recorded on a JEOL ECZ 400S spectrometer, with trimethylsilane (TMS) δH = 0 or residual protic solvent peak [$CDCl_3$, δ H = 7.26; D_2O, δ H = 4.80] as the internal standard. Chemical shifts are given in ppm (δ) and coupling constants (J) are given in Hertz (Hz). Jeol Delta v5.0.4. was used to analyse the NMR spectra. Zeta potential measurements were carried out using a Malvern Zetasizer nano ZS-series. Ultraviolet visible (UV–Vis) spectroscopy was carried out using a PerkinElmer spectrophotometer Lambda 25 and a Jenway 7315 spectrophotometer.

High resolution MS (HRMS) was measured at the Mass Spectrometry Centre, Faculty of Chemistry, University of Vienna utilizing a Bruker maXis UHR-TOF.

Transmission electron microscope (TEM) solid samples were dispersed in 100% ethanol unless otherwise stated. 5 μL drops of all samples were put onto carbon-coated copper grids and allowed to air dry. Images were obtained using Gatan Digital Micrograph software with an UltraScan 4000 digital camera attached to a Jeol 2010 TEM running at 200 kV.

The average diameter (D) and the size distribution of the nanoparticles were determined by using ImageJ software and by measuring 100 randomly selected nanoparticles in arbitrarily chosen areas of the TEM micrographs. The size distribution is reported as the standard deviation (σ) which is calculated according to the following formula: $\sigma = \{(D_i - D)^2 / (n - 1)\}^{1/2}$.

Thermogravimetric analysis (TGA) was performed using a Perkin Elmer TGA 4000 instrument in the temperature range of 30–700 °C under nitrogen atmosphere, at a heating rate of 10 °C min^{-1}.

2.2. Synthesis of ligands and nanoparticles

2.2.1. Synthesis of N-acetyl-O-ethyl-L-histidine

Ac-His-OH (350 mg, 1.78 mmol, 1 eq.) was charged with N_2 and suspended in dry EtOH (~10 mL). To this stirring suspension was added freshly distilled TMSCl (1.1 mL, 8.90 mmol, 5 eq.) dropwise. The suspension quickly turns into a solution and is stirred for a further 16 h at room temperature. The solvent was removed under reduced pressure and the resultant residue was dissolved in EtOH and triturated with Et_2O and hexane leading to an off-white solid. Yield 348 mg (87%), $C_{10}H_{15}N_3O_3$·HCl (261.1) Calcd.: C 45.90, H 6.16, N 16.06%. Found: C 45.63, H 6.27, N 15.96%. ^{1}H NMR (400 MHz, DMSO-d_6) δ = 9.00 (s, 1H, NC$_\varepsilon$*H*N), 8.50 (d, J = 8.0 Hz, 1H, N*H*CO), 7.39 (s, 1H, C$_\eta$*H*=C$_\gamma$), 4.49 (m, 1H, C$_\alpha$*H*COO), 4.04 (m, 2H, OC*H*$_2$CH$_3$), 3.07 (dd, J = 14.8, 5.2 Hz, 1H, C$_\beta$*H*$_a$H), 2.98 (dd, J = 15.2, 9.2 Hz, C$_\beta$*H*$_b$H), 1.78 (s, 3H, C*H*$_3$CO), 1.09 (t, J = 7.6 Hz, 3H, C*H*$_3$CH$_2$O) ppm. ^{13}C NMR (125 MHz, DMSO-d_6) δ = 171.2 (*C*OO), 170.1 (*C*ONH), 134.2 (N*C*$_\varepsilon$HN), 129.6 (*C*$_\gamma$ = C$_\eta$H), 117.5 (*C*$_\eta$H=C$_\gamma$), 61.3 (*C*H$_2$CH$_3$), 52.0 (*C*$_\alpha$HCOO), 26.5 (*C*$_\beta$H$_2$), 22.8 (*C*H$_3$CO), 14.5 (*C*H$_3$H$_2$) ppm.

2.2.2. Synthesis of 1,3-dimethyl-N-acetyl-O-ethyl-L-histidinium iodide, **1a**

Ac-His-OEt (300 mg, 1.3 mmol, 1 eq.), MeI (0.8 mL, 13.0 mmol, 10 eq.) and K_2CO_3 (718 mg, 5.2 mmol, 4 eq.) were suspended in MeCN (~20 mL). The reaction was refluxed for 14 h at 80 °C. The reaction mixture was cooled to room temperature and the solvent removed under reduced pressure. The resultant solid was dissolved in DCM and filtered. The filtrate was concentrated under reduced pressure and Et_2O was added to afford the product as a very hygroscopic off-white solid. Yield 425 mg (86%), $C_{12}H_{20}N_3O_3I$·1H$_2$O (381.1) Calcd: C 36.10, H 5.55, N 10.53%. Found: C 36.38, H 5.59, N 10.30%. ^{1}H NMR (400 MHz, $CDCl_3$) δ = 9.44 (s, 1H, NC$_\varepsilon$*H*N), 7.56 (d, J = 7.6 Hz, 1H, N*H*CO), 7.24 (s, 1H, C$_\eta$*H*=C$_\gamma$), 4.77 (m, 1H, C$_\alpha$*H*COO), 4.20 (m, 2H, OC*H*$_2$CH$_3$), 3.96 (NC*H*$_3$), 3.92 (NC*H*$_3$), 3.36 (dd, J = 16.0, 8.0 Hz, 1H, C$_\beta$*H*$_a$H), 3.20 (dd, J = 16.0, 4.0 Hz, C$_\beta$*H*$_b$H), 2.06 (s, 3H, C*H*$_3$CO), 1.27 (t, J = 7.6 Hz, 3H, C*H*$_3$CH$_2$O) ppm. ^{13}C NMR (125 MHz, $CDCl_3$) δ = 171.2 (*C*OO), 170.2 (*C*ONH), 136.8 (N*C*$_\varepsilon$HN), 132.1 (*C*$_\gamma$ = C$_\eta$H), 122.0 (*C*$_\eta$H=C$_\gamma$), 62.4 (*C*H$_2$CH$_3$), 50.7 (*C*$_\alpha$HCOO), 36.9 (N*C*H$_3$), 34.5 (N*C*H$_3$), 25.6 (*C*$_\beta$H$_2$), 23.4 (*C*H$_3$CO), 14.3 (*C*H$_3$H$_2$) ppm.

ESI-MS (m/z): Calcd. for $C_{12}H_{20}N_3O_3I[C_{12}H_{20}N_3O_3^+]$: 254.1504, Found: 254.1497.

2.2.3. Synthesis of chloride-1,3-dimethyl-N-acetyl-O-ethyl-L-histidin-2-ylidene gold(I), **2a**

Compound **1a** (400 mg, 1.04 mmol, 1 eq.) and Ag_2O (120 mg, 0.52 mmol, 0.5 eq.) were suspended in dry DCM (~5 mL) and stirred at room temperature for 1 h. To this reaction mixture [Au(SMe$_2$)Cl] (308 mg, 1.04 mmol, 1 eq.) was added. The reaction mixture was stirred for 1 h at room temperature. The resulting suspension was filtered through Celite and washed through with DCM. The filtrate was concentrated under reduced pressure, Et_2O and hexane were added to yield the product as an off-white solid. Yield 380 mg (75%), $C_{12}H_{19}N_3O_3AuCl$ (485.7) Calcd: C 29.67, H 3.94, N 8.65%. Found: C 29.45, H 3.83, N 8.63%. ^{1}H NMR (400 MHz, $CDCl_3$) δ = 6.71(s, 1H, C$_\eta$*H*=C$_\gamma$), 6.17 (d, J = 7.6 Hz, 1H, N*H*CO), 4.80 (m, 1H, C$_\alpha$*H*COO), 4.18 (m, 2H, OC*H*$_2$CH$_3$), 3.75 (NC*H*$_3$), 3.74 (NC*H*$_3$), 3.15 (dd, J = 13.6, 5.6 Hz, 1H, C$_\beta$*H*$_a$H), 3.02 (dd, J = 16.8, 7.2 Hz, C$_\beta$*H*$_b$H), 2.03 (s, 3H, C*H*$_3$CO), 1.27 (t, J = 7.2 Hz, 3H, C*H*$_3$CH$_2$O) ppm. ^{13}C NMR (125 MHz, $CDCl_3$) δ = 172.2 (N*C*$_\varepsilon$HN), 170.7 (*C*OO), 170.2 (*C*ONH), 129.3 (*C*$_\gamma$ = C$_\eta$H), 119.7 (*C*$_\eta$H=C$_\gamma$), 62.6 (*C*H$_2$CH$_3$), 51.2 (*C*$_\alpha$HCOO), 38.4 (N*C*H$_3$), 35.7 (N*C*H$_3$), 27.5 (*C*$_\beta$H$_2$), 23.3 (*C*H$_3$CO), 14.2 (*C*H$_3$H$_2$) ppm.

ESI-MS (m/z): Calcd. for $C_{12}H_{20}N_3O_3AuCl$ [bis complex – $C_{24}H_{38}N_6O_6Au^+$]: 703.2519, Found: 703.2511.

2.2.4. Synthesis of 1,3-isopropyl-N-acetyl-O-ethyl-L-histidinium iodide, ***1b***

Ac-His-OEt (600 mg, 2.6 mmol, 1 eq.), 2-iodopropane (5.2 mL, 52.0 mmol, 10 eq.) and K_2CO_3 (1.3 g, 10.6 mmol, 4 eq.) were suspended in MeCN (~40 mL). The reaction was refluxed for 72 h at 80 °C. The reaction mixture was cooled to room temperature and the solvent removed under reduced pressure. The resultant solid was dissolved in DCM and filtered. The filtrate was concentrated under reduced pressure and Et_2O was added to afford the product as a very hygroscopic off-white solid. Yield 732 mg (64%), $C_{16}H_{28}N_3O_3I$ (437.3) Calcd: C 43.94, H 6.45, N 9.61%. Found: C 44.43, H 6.74, N 9.70%. ^{1}H NMR (400 MHz, $CDCl_3$) δ = 9.60 (s, 1H, $NC_\varepsilon HN$), 7.73 (d, J = 8.0 Hz, 1H, N*H*CO), 7.25 (s, 1H, $C_\eta H{=}C_\gamma$), 4.88 (m, 1H, NC*H*$(CH_3)_2$), 4.75 (m, 1H, $C_\alpha H$COO), 4.59 (m, 1H, NC*H*$(CH_3)_2$), 4.20 (m, 2H, OCH_2CH$_3$), 3.43 (dd, J = 14.8, 5.2 Hz, 1H, $C_\beta H_a$H), 3.22 (dd, J = 16.0, 4.0 Hz, $C_\beta H_b$H), 2.04 (s, 3H, CH_3CO), 1.66 (m, 6H, NCH(CH_3)$_2$), 1.58 (d, J = 6.8 Hz, 6H, NCH(CH_3)$_2$), 1.26 (t, J = 6.8 Hz, 3H, CH_3CH$_2$O) ppm. ^{13}C NMR (125 MHz, $CDCl_3$) δ = 171.1 (*C*OO), 170.2 (*C*ONH), 132.9 (NC_εHN), 131.2 ($C_\gamma = C_\eta$H), 118.6 ($C_\eta{=}C_\gamma$), 62.3 (*C*H_2CH$_3$), 53.5 (N*C*H$(CH_3)_2$), 51.0 (N*C*H$(CH_3)_2$), 50.8 (C_αHCOO), 26.0 ($C_\beta H_2$), 23.8 (*C*H_3CO), 23.2 (4C, NCH(*C*H_3)$_2$), 14.3 (*C*H_3H_2) ppm.

ESI-MS (*m/z*): Calcd. for $C_{16}H_{28}N_3O_3I$[$C_{16}H_{28}N_3O_3^+$]: 310.2131, Found: 310.2138.

2.2.5. Synthesis of chlorido1,3-isopropyl-N-acetyl-O-ethyl-L-histidin-2-ylidene gold(I), ***2b***

Compound **1b** (280 mg, 0.64 mmol, 1 eq.) and Ag_2O (74 mg, 0.32 mmol, 0.5 eq.) were suspended in dry DCM (~5 mL) and stirred at room temperature for 1 h. To this reaction mixture was added [Au(SMe_2)Cl] (190 mg, 0.64 mmol, 1 eq.). The reaction mixture was stirred for 16 h at room temperature. The resulting suspension was filtered through Celite and washed through with DCM. The filtrate was concentrated under reduced pressure, Et_2O and hexane were added to yield the product as an orange solid. Yield 380 mg (75%), $C_{16}H_{27}N_3O_3AuCl{\cdot}1/4DCM$ (381.1) Calcd.: C 34.66, H 4.92, N 7.46%. Found: C 34.37, H 4.76, N 7.74%. ^{1}H NMR (400 MHz, $CDCl_3$) δ = 6.79 (s, 1H, $C_\eta H{=}C_\gamma$), 6.23 (d, J = 7.6 Hz, 1H, N*H*CO), 5.05 (m, 1H, NC*H*$(CH_3)_2$), 4.76 (m, 1H, $C_\alpha H$COO), 4.62 (m, 1H, NC*H*$(CH_3)_2$), 4.12 (m, 2H, OCH_2CH$_3$), 3.11 (dd, J = 15.6, 6.4 Hz, 1H, $C_\beta H_a$H), 3.04 (dd, J = 16.0, 6.8 Hz, $C_\beta H_b$H), 2.02 (s, 3H, CH_3CO), 1.73 (m, 6H, NCH(CH_3)$_2$), 1.40 (m, 6H, NCH(CH_3)$_2$), 1.22 (t, J = 7.2 Hz, 3H, CH_3CH$_2$O) ppm. ^{13}C NMR (125 MHz, $CDCl_3$) δ = 170.9 (NC_εHN), 170.2 (*C*OO), 167.9 (*C*ONH), 128.8 ($C_\gamma = C_\eta$H), 114.2 ($C_\eta{=}C_\gamma$), 62.3 (*C*H_2CH$_3$), 54.6 (N*C*H$(CH_3)_2$), 51.4 (N*C*H$(CH_3)_2$), 50.9 (C_αHCOO), 28.2 ($C_\beta H_2$), 24.0 (*C*H_3CO), 23.4 (4C, NCH(*C*H_3)$_2$), 14.2 (*C*H_3H_2) ppm.

ESI-MS (*m/z*): Calcd. for $C_{16}H_{27}N_3O_3AuCl$[$C_{16}H_{27}N_3O_3AuCl_2^-$]: 576.1095, Found: 576.1103.

2.2.6. Synthesis of ***3-NP(a)*** *by reduction of* ***2a*** *with* ^{t}***BuNH$_2$·BH$_3$***

Compound **2(a)** (10 mg, 0.02 mmol, 1 eq.) was dissolved in THF (1 mL) and stirred at high speed at room temperature. A separate solution of ^{t}BuNH$_2$·BH$_3$ (6 mg, 0.07 mmol, 3.6 eq.) was dissolved in THF (0.5 mL) and shaken till fully dissolved. The borane solution was added to the stirring gold solution. The reaction was left to stir at room temperature for 16 h. The solution turned a brown color and a drop of water was added to quench the reaction. The solvent was removed under reduced pressure yielding a black solid. The solid was re-dispersed in DCM and filtered. The filtrate had all solvent removed and dried under vacuum to yield product as a black powder. The remaining black solid was re-dispersed in THF and an aliquot taken drop-casted on a TEM grid to reveal the presence of nanoparticles 2.3 ± 0.4 (22.1%) nm. UV/Vis (DCM): λ_{max} = no plasmon band observed, ^{1}H NMR (400 MHz, $CDCl_3$) δ = 8.06 (d, J = 7.6 Hz, 1H, N*H*CO), 7.23(s, 1H, $C_\eta H{=}C_\gamma$), 4.74 (m, 1H, $C_\alpha H$COO), 4.21 (m, 2H, OCH_2CH$_3$), 3.83 (NCH_3), 3.80 (NCH_3), 3.30 (dd, J = 16.0, 8.8 Hz, 1H, $C_\beta H_a$H), 3.16 (dd, J = 16.0, 4.8 Hz, $C_\beta H_b$H), 2.06 (s, 3H, CH_3CO), 1.46 (s, 3H, CH_3CH$_2$O) ppm. ^{13}C NMR (125 MHz, $CDCl_3$) δ = 184.4 (NC_εN), 171.3 (*C*OO), 171.0 (*C*ONH), 131.1 ($C_\gamma = C_\eta$H), 121.4 ($C_\eta{=}C_\gamma$), 62.1 (*C*H_2CH$_3$), 52.8 (C_αHCOO), 38.1 (NCH_3), 35.5 (NCH_3), 26.6 ($C_\beta H_2$), 23.1 (*C*H_3CO), 14.2 (*C*H_3H_2) ppm.

2.2.7. Synthesis of ***4-NP(a)*** *by hydrolyzing* ***3-NP(a)***

3-NP(a) (20 mg) was suspended in EtOH (5 mL) and stirred at room temperature. NaOH (5 mg) was dissolved in water (5 mL) and added the nanoparticle suspension. The reaction mixture was then heated to 90 °C and stirred for 1 h. EtOH was removed under cool nitrogen flow as the reaction mixture cools down. Any precipitates are removed *via* filtering through cotton wool. The resulting filtrate was purified through dialysis (MWCO – 12,000–14,000 g mol^{-1}, wall thickness 20 μm) against MilliQ water, where the water was changed every 6 h over a 48-hour period. The solvent was removed under reduced pressure yielding a black solid and which could be re-dispersed again in dilute NaOH solutions. The remaining black solid was re-dispersed in H_2O and an aliquot taken drop-casted on a TEM grid to reveal the presence of nanoparticles 4.2 ± 1.2 (29.2%) nm. UV/Vis (DCM): λ_{max} = 515 nm, ^{1}H NMR (400 MHz, D_2O) δ = 6.84 (s, 1H, $C_\eta H{=}C_\gamma$), 4.30 (m, 1H, $C_\alpha H$COO), 3.65 (NCH_3), 3.64 (NCH_3), 3.00 (dd, J = 15.6, 5.2 Hz, 1H, $C_\beta H_a$H), 2.81 (dd, J = 15.6, 6.8 Hz, $C_\beta H_b$H), 1.86 (s, 3H, CH_3CO) ppm. ^{13}C NMR (125 MHz, $CDCl_3$) δ = 184.5 (NC_εN), 176.9 (*C*OO), 173.4 (*C*ONH), 130.6 ($C_\gamma = C_\eta$H), 120.9 ($C_\eta{=}C_\gamma$), 53.6 (C_αHCOO), 37.2 (NCH_3), 34.7 (NCH_3), 26.8 ($C_\beta H_2$), 21.9 (*C*H_3CO) ppm.

2.2.8. Synthesis of ***3-NP(b)*** *by reduction of* ***2b*** *with* ^{t}***BuNH$_2$·BH$_3$***

Compound **2b** (50 mg, 0.10 mmol, 1 eq.) was dissolved in THF (10 mL) and stirred at high speed at room temperature. A separate solution of ^{t}BuNH$_2$.BH$_3$ (30 mg, 0.36 mmol, 3.6 eq.) was dissolved in THF (2 mL) and shaken till fully dissolved. The borane solution was added to the stirring gold solution. The reaction was left to stir at room temperature for 16 h. The solution turned a brown color and a drop of water was added to quench the reaction. The solvent was removed under reduced pressure yielding a black solid. The solid was re-dispersed in DCM and filtered. The filtrate had all solvent removed and dried under vacuum to yield product as a black powder. The remaining black solid was re-dispersed in DCM and an aliquot taken drop-casted on a TEM grid to reveal the presence of nanoparticles 2.9 ± 0.5 (17.2%) nm. UV/Vis (DCM): λ_{max} = no plasmon band observed, ^{1}H NMR (400 MHz, $CDCl_3$) δ = 8.23 (d, J = 8.0 Hz, 1H, N*H*CO), 7.42 (s, 1H, $C_\eta H{=}C_\gamma$), 4.89 (m, 1H, NC*H*$(CH_3)_2$), 4.70 (m, 1H, $C_\alpha H$COO), 4.60 (m, 1H, NC*H*$(CH_3)_2$), 4.20 (m, 1H, OCH_2CH$_3$), 3.32 (dd, J = 16.0, 6.4 Hz, 1H, $C_\beta H_a$H), 3.20 (dd, J = 15.6, 4.8 Hz, $C_\beta H_b$H), 2.05 (s, 3H, CH_3CO), 1.75 (m, 6H, NCH(CH_3)$_2$), 1.49 (m, 6H, NCH(CH_3)$_2$), 1.46 (m, 3H, CH_3CH$_2$O) ppm. ^{13}C NMR (125 MHz, $CDCl_3$) δ = 179.8 (NC_εHN), 171.3 (*C*OO), 171.1 (*C*ONH), 130.4 ($C_\gamma = C_\eta$H), 116.2 ($C_\eta{=}C_\gamma$), 61.9 (*C*H_2CH$_3$), 54.8 (N*C*H$(CH_3)_2$), 51.3 (N*C*H$(CH_3)_2$), 49.9 (C_αHCOO), 27.9 ($C_\beta H_2$), 24.6 (*C*H_3CO), 23.4 (4C, NCH(*C*H_3)$_2$), 14.2 (*C*H_3H_2) ppm.

2.2.9. Synthesis of ***4-NP(b)*** *by hydrolyzing* ***3-NP(b)***

3-NP(b) (20 mg) was suspended in EtOH (5 mL) and stirred at room temperature. 0.1 M NaOH aqueous solution (5 mL) and added the nanoparticle suspension. The reaction mixture was then heated to 90 °C and stirred for 1 h. EtOH was removed under cool nitrogen flow as the reaction mixture cools down. Any precipitates are removed *via* filtering through cotton wool. The resulting filtrate was purified through dialysis (MWCO – 12,000–14,000 g mol^{-1}, wall thickness 20 μm) against MilliQ water, where the water was changed every 6 h over a 48-h period. The solvent was removed under reduced pressure yielding a black solid and could be re-dispersed again in dilute NaOH solutions. The remaining black solid was re-dispersed in H_2O and an aliquot taken drop-casted on a TEM grid to reveal the presence of nanoparticles 4.5 ± 0.7 (15.6%) nm. UV/Vis (DCM): λ_{max} = 531 nm, ^{1}H NMR (400 MHz, D_2O) δ = 6.98 (s, 1H, $C_\eta H{=}C_\gamma$), 4.85 (m, 1H, NC*H*$(CH_3)_2$), 4.48 (m, 1H, $C_\alpha H$COO), 4.26 (m, 1H, NC*H*$(CH_3)_2$, 3.10 (dd, J = 15.6, 4.0 Hz, 1H, $C_\beta H_a$H), 2.76 (dd, J = 15.6, 5.6 Hz, $C_\beta H_b$H), 1.78 (s, 3H, CH_3CO), 1.62 (d, J = 6.4 Hz,

3H, NCH(CH_3)$_2$), 1.55 (d, J = 6.8 Hz, 3H, NCH(CH_3)$_2$), 1.30 (d, J = 6.8 Hz, 6H, NCH(CH_3)$_2$) ppm. ^{13}C NMR (125 MHz, $CDCl_3$) δ = 179.6 (NC_εHN), 176.8 (COO), 173.1 ($CONH$), 130.5 (C_γ = C_ηH), 115.4 (C_ηH = C_γ), 54.5 (NCH(CH$_3$)$_2$), 53.7 (NCH(CH$_3$)$_2$), 49.4 (C_αHCOO), 27.4 ($C_\beta H_2$), 24.1 (CH_3CO), 23.8 (NCH(CH_3)$_2$), 22.7 (NCH(CH_3)$_2$), 22.3 (NCH(CH_3)$_2$), 21.9 (NCH(CH_3)$_2$) ppm.

2.3. Stability of *4-NP(a/b)* in various aqueous solutions

2.3.1. pH stability

A solution of **4-NP(a/b)** in MilliQ water was concentrated under reduced pressure and 50 µL was added to 1 mL of pH solutions ranging from pH = 1–13. pH solutions were prepared from 0.1 M HCl_{aq} and 0.1 M $NaOH_{aq}$ solutions, unless otherwise stated.

2.3.2. NMR studies of AuNPs

Glutathione (50 µL of 18 mM solution in D_2O) was added to make a total concentration of 2 mM and ^{1}H NMR spectra were recorded immediately after the addition, and then after 2 and 24 h.

3. Results and discussion

3.1. Synthesis and characterization

Histidine was selected as the NHC precursor due to the ease of converting the imidazole side chain into an imidazolium derivative [30]. Firstly the NHC-Au(I) complexes (**2a** and **2b**) were prepared from the respective imidazolium compounds (Scheme 1). As starting compound an N- and C-terminal protected histidine analog was used, namely Ac-L-His-OEt. Subsequent reactions of Ac-L-His-OEt with either methyl iodide or 2-propyl iodide yielded the desired imidazolium compounds **1a** and **1b** respectively. Reaction of **1a** and **1b** with Ag_2O and [Au(SMe_2)Cl] gives the Au(I) complexes **2a** and **2b** (Scheme 1).

Reduction of **2a** and **2b** with ^{t}BuNH$_2$·BH$_3$ led to the formation of a dark brown solution following quenching with water. The reaction was worked up and both **3-NP(a)** and **3-NP(b)** were isolated as black solids. No plasmon band was observed by UV–Vis spectroscopy for both samples, indicating the presence of small AuNPs. This was supported by TEM analysis of **3-NP(a)** revealing AuNPs with a size of 2.3 ± 0.4 (22.1%) nm (Fig. 1.b). TEM analysis of **3-NP(b)** revealed AuNPs with size of 2.9 ± 0.5 (17.2%) nm (Fig. 1.e). NMR spectroscopy was utilized to further demonstrate the formation of NHC stabilized AuNPs; ^{1}H and ^{13}C NMR spectroscopy supported the binding of the histidine NHC ligand on the AuNP surface, whereby the ^{13}C NMR spectrum showed that the carbene NHC peak had shifted from 172.2 ppm in the molecular species (**2a**) to 184.4 ppm in **3-NP(a)**. The down field shift of the coordinating carbon clearly demonstrates a change in the chemical environment suggesting the successful formation of AuNPs. A similar finding was observed for **3-NP(b)** where the carbene NHC peak had shifted from 170.9 ppm in the molecular species (**2b**) to 179.8 ppm in **3-NP(b)**.

To yield water dispersible NHC-AuNPs, compound **3-NP(a)** and **3-NP(b)** were saponified in a mixture of ethanol and 0.1 M $NaOH_{aq}$ solution and heated at 90 °C for 1 h. Upon completion the reaction mixture was purified through dialysis over a period of 24 h, giving rise to compounds **4-NP(a)** and **4-NP(b)**. UV–Vis analysis confirmed the presence of AuNPs exhibiting a surface plasmon band at 515 nm and 531 nm for **4-NP(a)** and **4-NP(b)** respectively (Fig. 1.a and d respectively), when dispersed in purified water. TEM analysis confirmed the presence of AuNPs with a size range of 4.2 ± 1.2 (29.2%) nm and 4.5 ± 0.7 (15.6%) nm for **4-NP(a)** and **4-NP(b)** respectively (Fig. 1.c and f respectively), demonstrating an increase in size of the AuNPs from **3-NP(a)** and **3-NP(b)**. Ripening of AuNPs upon heating is well documented for both thiol and NHC-stabilized systems [31–33]. Further, NMR analysis revealed, that the NHC ligand remained present at the gold surface as the carbene carbon signal was detected at 184.5 and 179.8 ppm (**4-NP(a)** and **4-NP(b)**) respectively. Additionally, the successful saponification was confirmed by ^{1}H and ^{13}C NMR spectroscopy through the absence of the ethyl ester peaks.

3.2. Thermogravimetric analysis

The extent of surface functionalization was estimated by thermogravimetric analysis (TGA). The organic content for **3-NP(a)** was found to be 55.9% and it decreased to 39.7% for **4-NP(a)** (Fig. 2.a). This observation is expected as the size of the AuNPs have increased between the two samples which suggests a greater gold to ligand ratio in **4-NP(a)**. The organic content for **3-NP(b)** was found to be 53.8% and it decreased to 46.3% for **4-NP(b)** (Fig. 2.b). The NHC:Au ratio calculated for **4-NP(a)** and **4-NP(b)** was found to be 0.57 and 0.60, respectively. Both samples appeared to be dispersible in aqueous solution suggesting the additional hydrophobic properties of the isopropyl groups of **4-NP(b)** have little effect in terms of solubility, however a significant difference in long term stability is observed with **4-NP(b)** showing greater susceptibility to degradation in solution. We postulate that this is due to the increased steric bulk of the isopropyl group as a similar observation was reported by Glorius and Ravoo where sterically demanding NHC-stabilized NPs showed higher susceptibility to degradation over NPs bearing less sterically demanding NHCs [34].

3.3. pH responsivity

Compounds **4-NP(a)** and **4-NP(b)** bear carboxylic acid groups, the dissociation of which afford electrostatic stabilization and water dispersibility to the NPs. Therefore, by decreasing the proportion of dissociated acid groups, pH dependent NP aggregation might be observed. To study the role of electrostatic stabilization, zeta potential measurements were taken for aqueous solutions of **4-NP(a)** and **4-NP(b)**. **4-NP(a)** and **4-NP(b)** were found to have zeta potentials of −24.3 mV and − 47.3 mV respectively in MilliQ water. This negative zeta potential is consistent with the presence of a deprotonated carboxylate moiety of the NHC ligand on the surface of the AuNPs. The isoelectric point was found to be pH 2.4 and pH 2.2 for **4-NP(a)** and **4-NP(b)** respectively.

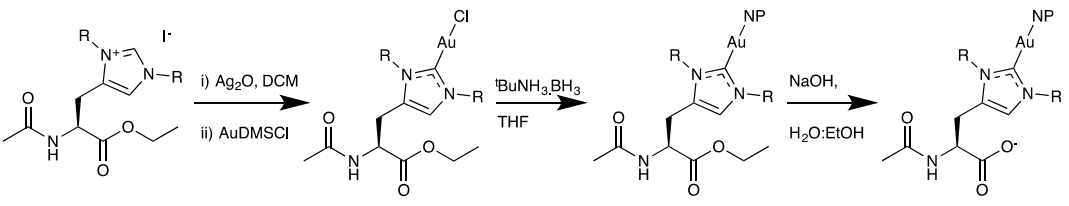

Scheme 1. Synthetic route employed to synthesize **4-NP(a/b)**.

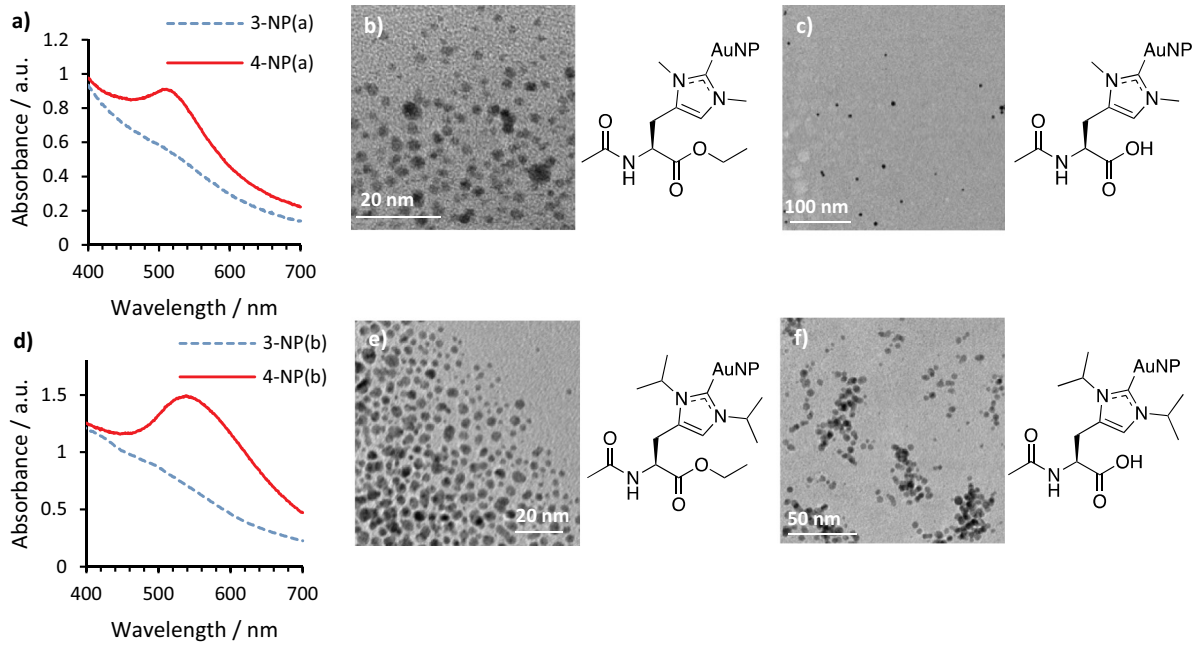

Fig. 1. a) UV–Vis spectra of **3-NP(a)** and **4-NP(a)**, TEM images of b) **3-NP(a)**, c) **4-NP(a)** with their respective chemical structures adjacent, d) UV–Vis spectra of **3-NP(b)** and **4-NP(b)**, and TEM images of e) **3-NP(b)** and f) **4-NP(b)** with their respective chemical structures adjacent.

In order to study any pH dependent aggregation, UV–Vis spectroscopy of **4-NP(a)** at varying pH values (pH = 1–13) was conducted. The sample showed a minimal shift of the plasmon band between pH ~ 3–13. However, a sharp shift of the surface plasmon band (Fig. 3.e) from 515 nm to 538 nm was observed at pH = 2.4. This shift can be attributed to the protonation of the carboxylic acid moiety and loss of electrostatic stabilization, whereby aggregation of the AuNPs is observed below pH = 2.4. This leads to a color change of the AuNP solution from red to purple (Fig. 3.a). Further studies of this phenomenon demonstrated that **4-NP(a)** could undergo reversible aggregation with the addition of dilute hydrochloric acid to promote aggregation and then the addition of dilute sodium hydroxide solution to disperse the AuNPs again (Fig. 3.a).

In contrast, when **4-NP(b)** was subjected to varying pH conditions, extensive ripening in both acidic (pH = 1–4) and basic solutions (pH = 9–13) is observed, leading to a shift of the plasmon band from 531 nm to 575 nm (Fig. 3.f) respectively. Indeed, **4-NP(b)** appears to be only stable in weakly acidic or basic solutions (pH = 5–8) (Fig. 3.f). This observed pH dependent ripening cannot only be explained by the different protonation states of the carboxylic acid moiety, as the carboxylic acid group is negatively charged above its pKa. We therefore assume, that the increased steric bulk of the isopropyl substituents increases the NP susceptibility to pH changes.

3.4. Stability testing

Having established a reliable synthetic route to water-soluble NHC stabilized AuNPs, we then investigated their stability in aqueous solutions under various environmental conditions. Stability was tested using a range of aqueous pH solutions (1 − 13), phosphate buffer solution (PBS, pH 7.4), NaCl (150 mM), and glutathione (GSH, 2 mM). Furthermore, long term stability was examined in water. The stability was monitored by UV–Vis spectroscopy as any changes in the plasmon band of AuNPs (intensity as well as a shift the plasmon band) are indicative of a change of the nature of the investigated AuNPs.

The long term stability of **4-NP(a)** was found to be very good; an aqueous solution of **4-NP(a)** stored over 72 days in the laboratory at room temperature showed only a small shift of the plasmon band, suggesting a modest ripening of the particles. In contrast **4-NP(b)** showed a change in the plasmon band after only 7 days and after

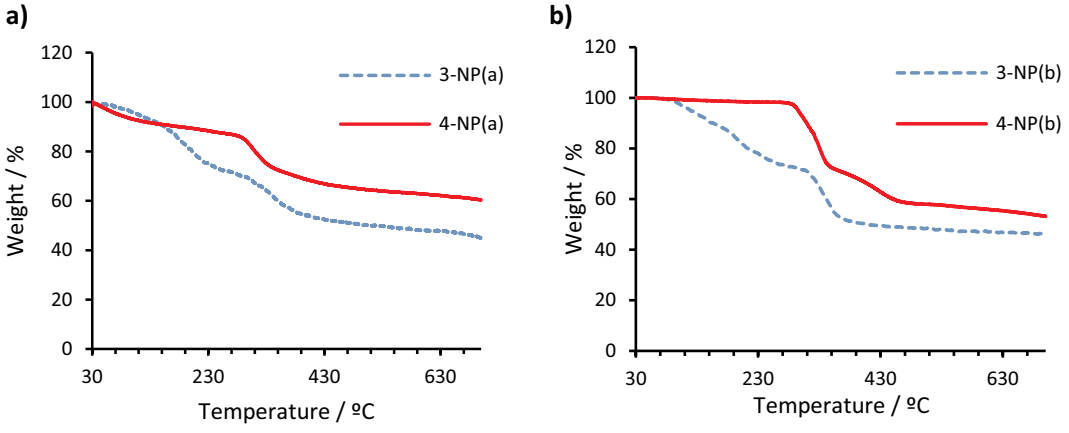

Fig. 2. a) TGA of **3-NP(a)** and **4-NP(a)** and b) TGA of 3-NP(b) and 4-NP(a).

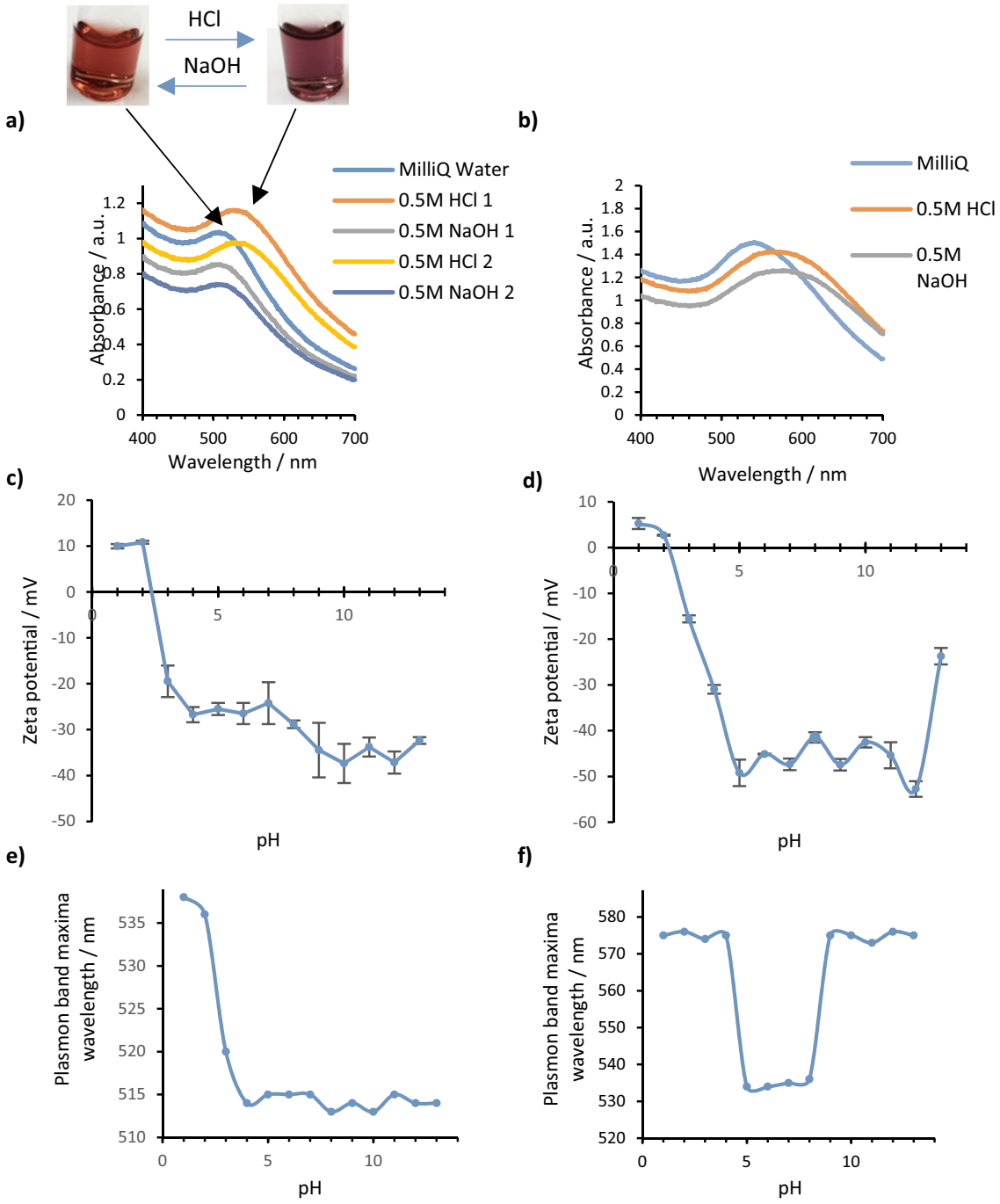

Fig. 3. a) UV–Vis absorption spectra of 0.3 mg/mL of **4-NP(a)** in aqueous solutions showing reversible aggregation and redispersibility of the AuNPs depending on the pH, b) UV–Vis absorption spectra of 0.60 mg/mL of **4-NP(b)** in aqueous solutions showing no reversible aggregation and redispersibility of the AuNPs depending on the pH, c) zeta potential of **4-NP(a)** in varying aqueous pH solutions, d) zeta potential of **4-NP(b)** in varying aqueous pH solutions, e) UV–vis absorbance spectra of **4-NP(a)** at varying pH and f) UV–Vis absorbance spectra of **4-NP(b)** at varying pH.

14 days a substantial difference in the plasmon band can be seen, which can be attributed to extensive ripening of the AuNPs.

Next we tested the stability of **4-NP(a/b)** in the presence of electrolytes [35,36]. An aqueous solution of 150 mM NaCl was chosen to simulate physiologically relevant saline concentrations, and the AuNPs were monitored by UV–Vis spectroscopy. **4-NP(b)** was stable for 1 day in the electrolyte solution, after which the surface plasmon band is absent and the AuNPs have clearly degraded (Fig. 4.f). In contrast, **4-NP (a)** was found to be highly stable in the electrolyte solution, after 14 days a minor shift of the plasmon band is observed which suggests a minor ripening of the AuNPs, but after 36 days the plasmon band shows signs of AuNP degradation due to broadening and lowering of the plasmon band (Fig. 4.e).

When **4-NP(a)** was exposed to phosphate buffer solution (pH 7.4) the AuNPs remain well-dispersed and a minor shift of the plasmon band is observed (Fig. 4.e), indicating modest ripening. **4-NP(a)** appears to be stable for 14 days without degradation, but after 36 days the AuNPs show signs of degradation. In comparison **4-NP(b)** was found to undergo immediate ripening of the AuNPs with broadening of the plasmon band (Fig. 4.d) and after only 24 h the AuNPs had completely degraded and sedimented out of the solution.

We further studied the stability of **4-NP(a)** and **4-NP(b)** in the

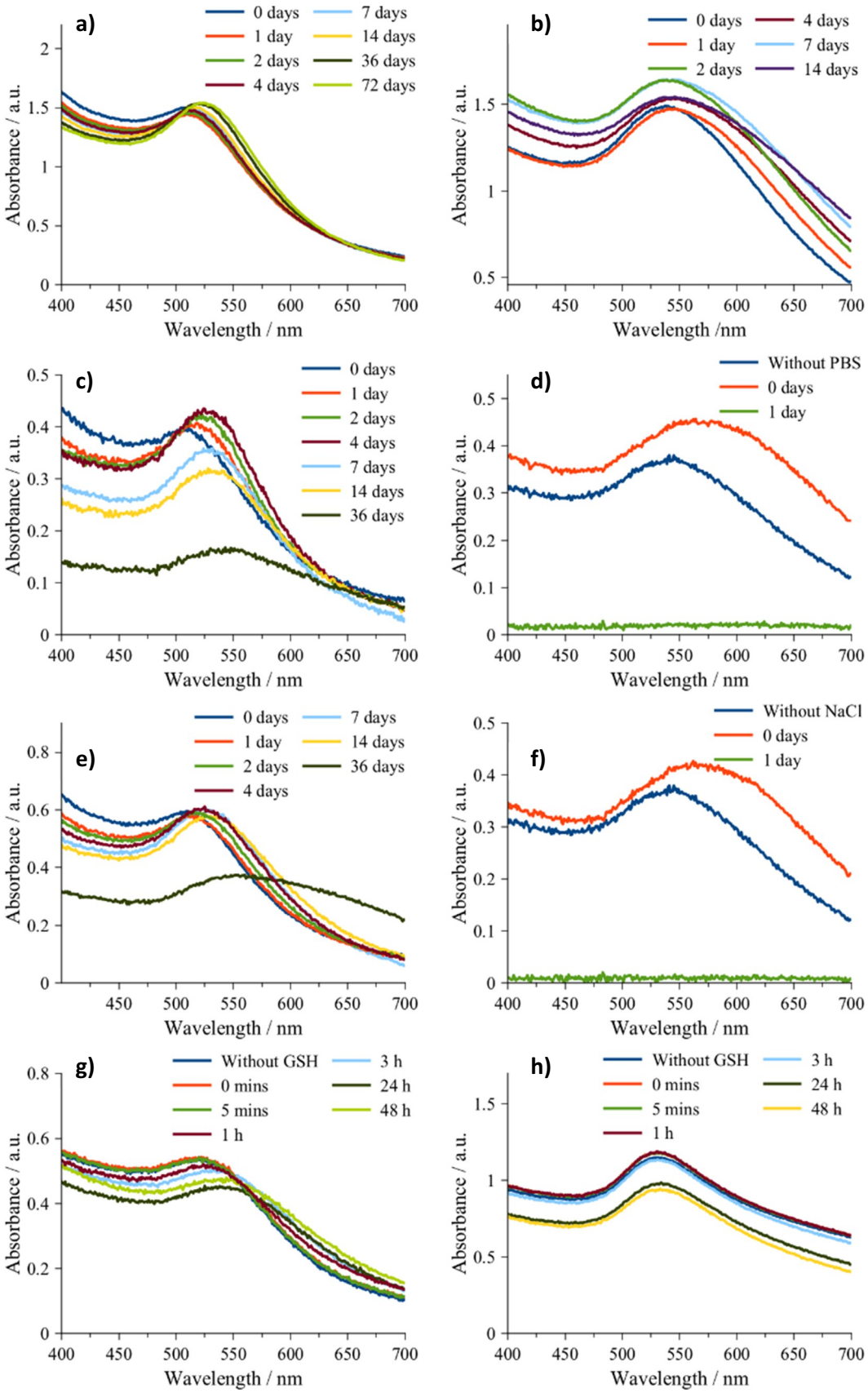

Fig. 4. a) 0.45 mg/mL of **4-NP(a)** in MilliQ water, b) 0.70 mg/mL of **4-NP(b)** in MilliQ water, c) 0.10 mg/mL of **4-NP(a)** in PBS (pH 7.4), d) 0.20 mg/mL of **4-NP(b)** in PBS (pH 7.4), e) 0.15 mg/mL of **4-NP(a)** in 150 mM NaCl, f) 0.20 mg/mL of **4-NP(b)** in 150 mM NaCl, g) 0.15 mg/mL of **4-NP(a)** in 2 mM GSH at pH 8 and h) 0.55 mg/mL of **4-NP(b)** in 2 mM GSH at pH 8.

presence of the biomolecule glutathione (GSH), because the thiol-bearing GSH is well known to cause AuNP degradation [23,24]. GSH is typically found in the body at concentrations ranging from 0.5 to 10.0 mM [37,38]; as such a GSH concentration of 2 mM was utilized. Initial stability studies of **4-NP(a)** and **4-NP(b)** in GSH demonstrated that they were not stable (Figs. S19 and S20 respectively, ESI). However, GSH bears free carboxylic acid groups and the initial solution of GSH was found to have a pH of 3. Therefore, to preclude the effect of low pH on the nanoparticles, GSH stability studies were also studied following a procedure reported by Crudden [24], in which the solution pH was adjusted to pH 8. Under these conditions **4-NP(a)** was found to be stable for up to 48 h with only a minor shift of the plasmon band being observed (Fig. 4.g). In contrast, for **4-NP(b)** the intensity of the plasmon band decreases after 24 h indicating some degradation/aggregation of the AuNPs although no shift in the plasmon band was observed (Fig. 4.g).

We further studied the stability against GSH, of both **4-NP(a)** and **4-NP(b)** through ^{1}H NMR to demonstrate the structural stability of the AuNPs (Figs. S21 and S22 respectively, ESI). All NMR spectra of both AuNPs showed no change in the nature of the AuNPs with regards to the NHC ligand. Throughout the NMR experiments the AuNPs were dispersed in solution. Suggesting the NHC ligands in both AuNP samples do not get displaced by the thiol GSH ligand.

4. Conclusion

In conclusion, we describe a method drawing from a naturally occurring molecule to generate NHC ligands for the stabilization of AuNPs. L-Histidine was utilized as an NHC precursor yielding well-defined organometallic NHC-Au(I) complexes. Two histidine derived ligands were synthesized with either methyl or isopropyl substituents on the imidazole ring nitrogens. This allowed us to study the influence of sterically more demanding isopropyl group on the stability of the resulting AuNPs. Therefore, methyl and isopropyl Au(I) NHC gold complexes were synthesized and subsequently reduced to AuNPs using $^{t}BuNH_2{\cdot}BH_3$ as reducing agent. The resulting AuNPs bore an ethyl ester which was saponified to give rise to water soluble AuNPs. **4-NP(a)** was found to possess pH responsivity and demonstrated relatively good stability in a variety of biologically relevant solutions (*e.g.* PBS, NaCl, GSH). In contrast the isopropyl derivative was found to be much less stable in all tested biologically relevant solutions. High stability was observed up to 72 days and relatively good stability to ionic strengths of biological relevant media was observed for **4-NP(a)**, but the isopropyl (**4-NP(b)**) was found to be much less stable. We postulate that this is due to the increased steric bulk of the isopropyl group as a similar observation was reported by Glorius and Ravoo where sterically demanding NHC-stabilized NPs showed higher susceptibility to degradation over NPs bearing less sterically demanding NHCs [34]. We are currently expanding this work towards NHC-AuNPs which demonstrate pH response under mildly acidic or basic conditions (pH 5–8) as well as NPs which are less susceptible to GSH degradation.

Abbreviations

AuNP	gold nanoparticle
GSH	glutathione
HRMS	high resolution mass spectrometry
NHC	N-heterocyclic carbene
NMR	nuclear magnetic resonance
NP	nanoparticle
PBS	phosphate buffered saline
PEG	polyethylene glycol
TEM	transmission electron microscope
TGA	thermogravimetric analysis
TMS	tetramethylsilane
UV–Vis	ultraviolet-visible

Acknowledgements

MRR thanks the University of Vienna for financial support. JC thanks the University of Hull for providing the financial support to carry out this work. AJY thanks the University of Hull for the provision of a University Scholarship.

Appendix A. Supplementary data

Supplementary data to this article can be found online at https://doi.org/10.1016/j.jinorgbio.2019.110707.

References

[1] A. Roucoux, J. Schulz, H. Patin, Reduced transition metal colloids: a novel family of reusable catalysts? Chem. Rev. 102 (2002) 3757–3778, https://doi.org/10.1021/cr010350j.
[2] R.J. White, R. Luque, V.L. Budarin, J.H. Clark, D.J. MacQuarrie, Supported metal nanoparticles on porous materials. Methods and applications, Chem. Soc. Rev. 38 (2009) 481–494, https://doi.org/10.1039/b802654h.
[3] L.D. Pachón, G. Rothenberg, Transition-metal nanoparticles: synthesis, stability and the leaching issue, Appl. Organomet. Chem. 22 (2008) 288–299, https://doi.org/10.1002/aoc.1382.
[4] C. Burda, X. Chen, R. Narayanan, M.A. El-Sayed, Chemistry and properties of nanocrystals of different shapes, Chem. Rev. 105 (2005) 1025–1102, https://doi.org/10.1021/cr030063a.
[5] D. Astruc, F. Lu, J.R. Aranzaes, Nanoparticles as recyclable catalysts: the frontier between homogeneous and heterogeneous catalysis, Angew. Chem. Int. Ed. 44 (2005) 7852–7872, https://doi.org/10.1002/anie.200500766.
[6] K. Saha, S.S. Agasti, C. Kim, X. Li, V.M. Rotello, Gold Nanoparticles in Chemical and Biological Sensing, American Chemical Society, 2012, https://doi.org/10.1021/cr2001178.
[7] L. Dykman, N. Khlebtsov, Gold nanoparticles in biomedical applications: recent advances and perspectives, Chem. Soc. Rev. 41 (2012) 2256–2282, https://doi.org/10.1039/c1cs15166e.
[8] E.C. Dreaden, A.M. Alkilany, X. Huang, C.J. Murphy, M.A. El-Sayed, The golden age: gold nanoparticles for biomedicine, Chem. Soc. Rev. 41 (2012) 2740–2779, https://doi.org/10.1039/c1cs15237h.
[9] M. Thompson, A.E. Nel, P. Somasundaran, L. Mädler, F. Klaessig, D. Velegol, E.M.V. Hoek, V. Castranova, T. Xia, Understanding biophysicochemical interactions at the nano–bio interface, Nat. Mater. 8 (2009) 543–557, https://doi.org/10.1038/nmat2442.
[10] N.L. Rosi, C.A. Mirkin, Nanostructures in biodiagnostics, Chem. Rev. 105 (2005) 1547–1562, https://doi.org/10.1021/cr030067f.
[11] P. Alivisatos, The use of nanocrystals in biological detection, Nat. Biotechnol. 22 (2004) 47–52, https://doi.org/10.1038/nbt927.
[12] E. Oh, K. Susumu, A.J. Mäkinen, J.R. Deschamps, A.L. Huston, I.L. Medintz, Colloidal stability of gold nanoparticles coated with multithiol-poly(ethylene glycol) ligands: importance of structural constraints of the sulfur anchoring groups, J. Phys. Chem. C 117 (2013) 18947–18956, https://doi.org/10.1021/jp405265u.
[13] N.T.K. Thanh, L.A.W. Green, Functionalisation of nanoparticles for biomedical applications, Nano Today 5 (2010) 213–230, https://doi.org/10.1016/j.nantod.2010.05.003.
[14] M.M. Maye, W. Zheng, F.L. Leibowitz, N.K. Ly, C.J. Zhong, Heating-induced evolution of thiolate-encapsulated gold nanoparticles: a strategy for size and shape manipulations, Langmuir 16 (2000) 490–497, https://doi.org/10.1021/la990892k.
[15] N. Bhatt, P.-J.J. Huang, N. Dave, J. Liu, Dissociation and degradation of thiol-modified DNA on gold nanoparticles in aqueous and organic solvents, Langmuir 27 (2011) 6132–6137, https://doi.org/10.1021/la200241d.
[16] L. Srisombat, A.C. Jamison, T.R. Lee, Stability: a key issue for self-assembled monolayers on gold as thin-film coatings and nanoparticle protectants, Colloids Surf. A Physicochem. Eng. Asp. 390 (2011) 1–19, https://doi.org/10.1016/j.colsurfa.2011.09.020.
[17] M.R. Narouz, C.-H. Li, A. Nazemi, C.M. Crudden, Amphiphilic N-heterocyclic carbene-stabilized gold nanoparticles and their self-assembly in polar solvents, Langmuir 33 (2017) 14211–14219, https://doi.org/10.1021/acs.langmuir.7b02248.
[18] J. Vignolle, T.D. Tilley, N-heterocyclic carbene-stabilized gold nanoparticles and their assembly into 3D superlattices, Chem. Commun. 21 (2009) 7230–7232, https://doi.org/10.1039/b913884f.
[19] A. Ferry, K. Schaepe, P. Tegeder, C. Richter, K.M. Chepiga, B.J. Ravoo, F. Glorius, Negatively charged N-heterocyclic carbene-stabilized Pd and Au nanoparticles and efficient catalysis in water, ACS Catal. 5 (2015) 5414–5420, https://doi.org/10.1021/acscatal.5b01160.
[20] R. Ye, A.V. Zhukhovitskiy, R.V. Kazantsev, S.C. Fakra, B.B. Wickemeyer, F.D. Toste, G.A. Somorjai, Supported Au nanoparticles with N-heterocyclic carbene ligands as active and stable heterogeneous catalysts for lactonization, J. Am. Chem. Soc. 140 (2018) 4144–4149, https://doi.org/10.1021/jacs.8b01017.
[21] N. Bridonneau, L. Hippolyte, D. Mercier, D. Portehault, M. Desage-El Murr, P. Marcus, L. Fensterbank, C. Chanéac, F. Ribot, N-Heterocyclic carbene-stabilized gold nanoparticles with tunable sizes, Dalton Trans. 47 (2018) 6850–6859, https://

doi.org/10.1039/c8dt00416a.
[22] S. Roland, X. Ling, M.-P. Pileni, *N*-Heterocyclic carbene ligands for Au nanocrystal stabilization and three-dimensional self-assembly, Langmuir 32 (2016) 7683–7696, https://doi.org/10.1021/acs.langmuir.6b01458.
[23] M.J. MacLeod, J.A. Johnson, PEGylated *N*-heterocyclic carbene anchors designed to stabilize gold nanoparticles in biologically relevant media, J. Am. Chem. Soc. 137 (2015) 7974–7977, https://doi.org/10.1021/jacs.5b02452.
[24] K. Salorinne, R.W.Y. Man, C.H. Li, M. Taki, M. Nambo, C.M. Crudden, Water-soluble N-heterocyclic carbene-protected gold nanoparticles: size-controlled synthesis, stability, and optical properties, Angew. Chem. Int. Ed. 56 (2017) 6198–6202, https://doi.org/10.1002/anie.201701605.
[25] E.A. Baquero, S. Tricard, J.C. Flores, E. De Jesffls, B. Chaudret, E. de Jesús, B. Chaudret, Highly stable water-soluble platinum nanoparticles stabilized by hydrophilic N-heterocyclic carbenes, Angew. Chem. Int. Ed. 53 (2014) 13220–13224, https://doi.org/10.1002/anie.201407758.
[26] A. Rühling, K. Schaepe, L. Rakers, B. Vonhören, P. Tegeder, B.J. Ravoo, F. Glorius, Modular bidentate hybrid NHC-thioether ligands for the stabilization of palladium nanoparticles in various solvents, Angew. Chem. Int. Ed. 55 (2016) 5856–5860, https://doi.org/10.1002/anie.201508933.
[27] J. Song, J. Kim, S. Hwang, M. Jeon, S. Jeong, C. Kim, S. Kim, "Smart" gold nanoparticles for photoacoustic imaging: an imaging contrast agent responsive to the cancer microenvironment and signal amplification: via pH-induced aggregation, Chem. Commun. 52 (2016) 8287–8290, https://doi.org/10.1039/c6cc03100e.
[28] K.-H. Lui, S. Li, X. Li, C. Hiu-Ling Hung, W.-S. Lo, W. Chi-Shing Tai, X. Hu, W.-T. Wong, T.-H. Tsoi, Y.-J. Gu, pH-responsive targeted gold nanoparticles for in vivo photoacoustic imaging of tumor microenvironments, Nanoscale Adv. 1 (2018) 554–564, https://doi.org/10.1039/c8na00190a.
[29] T.N. Hooper, C.P. Butts, M. Green, M.F. Haddow, J.E. McGrady, C.A. Russell, Synthesis, structure and reactivity of stable homoleptic gold(I) alkene cations, Chem. Eur. J. 15 (2009) 12196–12200, https://doi.org/10.1002/chem.200902566.
[30] F. Schmitt, K. Donnelly, J.K. Muenzner, T. Rehm, V. Novohradsky, V. Brabec, J. Kasparkova, M. Albrecht, R. Schobert, T. Mueller, Effects of histidin-2-ylidene vs. imidazol-2-ylidene ligands on the anticancer and antivascular activity of complexes of ruthenium, iridium, platinum, and gold, J. Inorg. Biochem. 163 (2016) 221–228, https://doi.org/10.1016/j.jinorgbio.2016.07.021.
[31] R.W.Y. Man, C.-H. Li, M.W.A. MacLean, O.V. Zenkina, M.T. Zamora, L.N. Saunders, A. Rousina-Webb, M. Nambo, C.M. Crudden, Ultra stable gold nanoparticles modified by bidentate N-heterocyclic carbene ligands, J. Am. Chem. Soc. 140 (2017) 1576–1579, https://doi.org/10.1021/jacs.7b08516.
[32] B.L.V. Prasad, S.I. Stoeva, C.M. Sorensen, K.J. Klabunde, Digestive ripening of thiolated gold nanoparticles: the effect of alkyl chain length, Langmuir 18 (2002) 7515–7520, https://doi.org/10.1021/la020181d.
[33] L.O. Srisombat, S. Zhang, T. Randall Lee, Thermal stability of mono-, bis-, and tris-chelating alkanethiol films assembled on gold nanoparticles and evaporated "flat" gold, Langmuir 26 (2010) 41–46, https://doi.org/10.1021/la902082j.
[34] C. Richter, K. Schaepe, F. Glorius, B.J. Ravoo, Tailor-made N-heterocyclic carbenes for nanoparticle stabilization, Chem. Commun. 50 (2014) 3204–3207, https://doi.org/10.1039/c4cc00654b.
[35] T. Laaksonen, P. Ahonen, C. Johans, K. Kontturi, Stability and electrostatics of mercaptoundecanoic acid-capped gold nanoparticles with varying counterion size, ChemPhysChem 7 (2006) 2143–2149, https://doi.org/10.1002/cphc.200600307.
[36] R. Pamies, J.G.H. Cifre, V.F. Espín, M. Collado-González, F.G.D. Baños, J.G. De La Torre, Aggregation behaviour of gold nanoparticles in saline aqueous media, J. Nanopart. Res. 16 (2014) 2376, , https://doi.org/10.1007/s11051-014-2376-4.
[37] P. Maher, The effects of stress and aging on glutathione metabolism, Ageing Res. Rev. 4 (2005) 288–314, https://doi.org/10.1016/j.arr.2005.02.005.
[38] G.K. Balendiran, R. Dabur, D. Fraser, The role of glutathione in cancer, Cell Biochem. Funct. 22 (2004) 343–352, https://doi.org/10.1002/cbf.1149.